Hindawi
Shock and Vibration
Volume 2017, Article ID 4163045, 16 pages
https://doi.org/10.1155/2017/4163045

Research Article

Wind-Induced Response of an L-Shaped Cable Support Glass Curtain Wall

Yan Yu,[1] Tao Liu,[2] Qilin Zhang,[1] and Bin Yang[1]

[1]*Department of Structural Engineering, Tongji University, Shanghai 200092, China*
[2]*Department of Civil Engineering, Xiamen University, Xiamen 361005, China*

Correspondence should be addressed to Tao Liu; taoliu@xmu.edu.cn

Received 7 March 2017; Revised 15 May 2017; Accepted 29 May 2017; Published 13 August 2017

Academic Editor: Filippo Ubertini

Due to its flexibility, cable support glass curtain wall is sensitive to wind loads and its wind-induced dynamic response has attracted more and more attention recently. However, the wind-resistant study for this kind of structure mainly focuses on single-layer plane cable support curtain walls but is rare on irregular ones. In this paper, the wind-induced response of an L-shaped cable support glass curtain wall is analyzed. In order to truly reflect the force transmission, a finite element model of curtain wall is established to ensure collaborative deformation between glass and cable, including glass panel, cable, sealant, and claw connection. Time-domain vibration analysis of the curtain wall is carried out with the random sequence of multinode fluctuating wind velocity time history simulated by autoregressive linear filtering method based on Kaimal wind velocity spectrum. Four wind flow directions are specified, namely, 0°, 15°, 30°, and 45°, to analyze the wind-induced dynamic response of this structure with consideration of the fluid-structure interaction effect. Finally, the deflection of the glass surface is studied by statistical analysis of displacement so as to obtain the wind vibration coefficient suitable for structural design of practical projects, and the variation of cable force is investigated as well.

1. Introduction

Glass curtain wall is a structural form combining the ancient art style and the modern architecture technology, which has been a symbol of the international modern metropolis [1]. Cable support glass curtain wall that consists of cables and glass panels reflects the development trend of large-scale curtain walls [2]. Due to its simple force transmission, lightweight construction style, good visual permeability, and convenient construction process, it has been widely used around the world, such as in China Maritime Museum in Shanghai and Time Warner Center in New York.

Although the structural performance of cable net glazing facades under impact, blast, or seismic loads (including both experiments and detailed FEM) has been widely investigated by researchers [3–6], wind performance of cable net glazing facades is dominant, especially in high-rise buildings. In general, wind load is directly applied to the tempered glass panels, which serves as the building envelope, and then transferred to a supporting structure by the stainless steel claw connection. To develop a more transparent, safe, and flexible building envelope, glass panels are connected with sealants to maintain integrity without an aluminum frame. A cable network system is usually used as a supporting structure, in which cable ends are anchored to the main structure and the cables can bear the load after having been prestressed. In this way, the whole structure remains in tension and thus avoids the buckle problem in structural design, which fully realizes the full play of mechanical properties of cables and saves steel consumption.

Under fluctuating wind load, the cable support glass curtain will have a large deformation and severe vibration due to its lightweight and flexibility, which will in turn affect the wind pressure distribution on the structural surface, namely, the fluid-structure interaction effect. In addition, the cable net structure has dense and coupled vibration modes and is of obvious geometric nonlinearity. Consequently, it is impossible to estimate the wind-induced response according to low-order vibration modes alone, because they are normally adequate for the analysis of high-rise buildings and

those classic analytical formulas cannot be directly applied as well. So far, even for European countries with broader application of cable support glass curtain wall, there is still no mature design theory but just some enterprise standards; thus, research institutions are stepping up to make this construction technology more complete.

The study on the dynamic response of structures under fluctuating wind load mainly adopts the frequency-domain method and time-domain method [7–9]. The former establishes the structural response spectrum directly based on the stochastic vibration theory. This method is suitable for analysis of linear and weak nonlinear structures because of its lower cost, easy application, and clear physical meaning. The latter simulates the dynamic response of a structure by a step-by-step integral method, namely, directly applying fluctuating wind velocity time history to the structure. This method can obtain higher accuracy and is more suitable for structures with dense vibration frequencies, large flexibility, and significant nonlinear characteristics such as spatial structure and particular large-scale structure.

For the wind-induced vibration response study of a single-layer cable structure, the frequency-domain method requires the average wind pressure position as the initial computing position instead of the initial state of the structure. In this situation, the single-layer cable is in the balance position and the nonlinear deformation is almost complete. In addition, the structure vibrates slightly around this location under fluctuating wind with weak geometric nonlinearity. Although the frequency-domain method can be used for wind-induced vibration response study, there is certain error due to the weak geometric nonlinearity. Therefore, time-history analysis is usually adopted so as to obtain a more accurate wind-induced vibration response.

The frequency-domain method mainly involves the selection of vibration modes and their coupling relationship. Wu et al. [10] investigated the wind-induced response of the monolayer cable net subjected to fluctuating wind loads with frequency-domain method and found that the first mode dominates the wind-induced response significantly in all the modes, and the modes contributing to the wind-induced responses prominently are distributed in a narrow band of low-order modes. Xu et al. [11] adopted viscoelastic dampers (VEDs) to reduce the wind-induced dynamic responses of a 75-meter-high chimney. A simulation method for the stochastic wind field based on the modified Fourier spectrum was proposed and it was concluded that the accuracy of the modified Fourier spectrum method (MFSM) was greatly improved when compared with the spectrum representation method of simulating the stochastic wind field. Based on proper orthogonal decomposition (POD) and pseudoexcitation methods, Zhao et al. [12] proposed a new method to analyze wind-induced response in frequency domain for a conch-shaped single-layer lattice shell. Hernandez et al. [13] carried out the frequency-domain analysis of the performance of a wind turbine that is placed in a mountainous complex terrain, so as to estimate the magnitude squared of the frequency response of the system and to estimate the average value of the magnitude squared of the frequency response.

Liu et al. [14] analyzed wind-induced vibration response of point-supported glass curtain wall cable truss structure through time-domain method and ANSYS software. Feng et al. [15] used the continuous membrane theory to construct the nonlinear vibration differential equation of the cable net and adopted the harmonic balance method to solve the analytic formula of the nonlinear frequency. Zhang and Ju [16] established a finite element model of a four-circuit tower consisting of steel tubes and angle steels and conducted dynamic response analysis of 10 samples under two kinds of wind field, in which Davenport wind speed spectrum and Shiotani coherence function were, respectively, used to simulate wind speed time history. Zhang et al. [17] illustrated the dynamic properties of the non-fully symmetric Geiger cable dome. Linear filter autoregressive (AR) method was used to obtain the horizontal and vertical fluctuating wind velocity time-history curves of the cable dome, and the shape coefficient of the cable dome was simulated by CFD method. Cai et al. [18] investigated the wind-induced response behavior of the single-layer cable net supported glass curtain walls in cooperation with glass panels. The wind speed time history was firstly developed with MATLAB before time-history analysis of cable net with glass and cable net alone. The results showed that the influence of glass panels on the node's largest deflection is great but on the cable force is small. Wang et al. [19] performed FEM analysis and experimental study on monolayer cable net for glass facades and discussed the influence of glass stiffness and nodal constraint on its dynamic properties.

The study on wind vibration mechanism of cable support glass curtain wall is still in its initial stage, without a theoretical framework, and still needs a large amount of analysis from different aspects. Since the equivalent thickness of glass is less than 20 mm and the cable diameter is also small, it is difficult to achieve the similarity conditions in wind tunnel tests when large structural deformations interact with fluid flow. So, wind-induced response of an L-shaped cable support glass curtain wall is analyzed by numerical simulation in this paper. For the sake of simplification, the catenary effects are not considered here and will be investigated in the future. In order to truly reflect the force transmission, a finite element model of curtain wall, including glass panel, cable, sealant, and claw connection, is established to ensure collaborative deformation between glass panels and cables. According to structural symmetry, four wind flow directions are specified, namely, 0°, 15°, 30°, and 45°, to analyze the wind-induced dynamic response of this structure with consideration of the fluid-structure interaction effect. Finally, wind-induced response is studied to obtain the wind vibration coefficient suitable for structural design of practical projects.

2. Structural Model

A building located in Fuzhou (China) is taken as research object in this study, where the construction site belongs to type B, the design wind pressure with 50-year return period is 0.7, and the design wind velocity is 33.5 m/s. The main building has 18 stories, which is 83 m in height and 44.5 m in both length and width. The cable support glass curtain wall

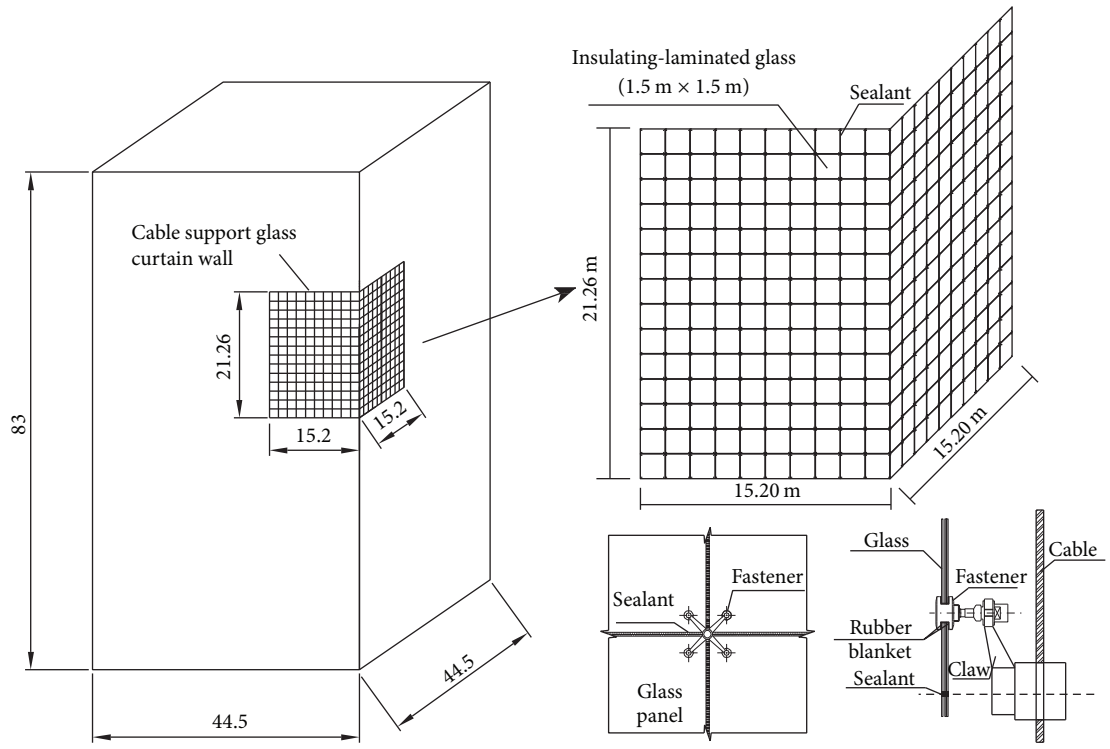

Figure 1: Structural layout (m).

locates in the corner of 10–14 stories, with a height of 21.26 m and a length of 15.20 m in each side, as shown in Figure 1. The glass curtain wall consists of four parts, namely, prestressed cables, claw connections, glass panels, and sealants. Glass panels are connected by the silicone sealant, while the corners of glass panels are connected with cables through claws. The connection between the glass panels and the claw is only hinged in the direction perpendicular to glass panel and there are no other restrictions in the plane of glass face. The glass panels are hinged with an embedded part and the main structure through an anchorage plate, and both ends of the cables are hinged to the main structure. Based on the above structural design, the force transmission path is: wind load > glass panel > claw connection > prestressed cable > the main structure.

The main element of the cable supported glass curtain is the prestressed cable, which transfers the wind force applied on the glass panel to the main structure by claw connections. Under wind loads, glass panels work with the cables in the following three ways.

(1) Mass of Glass Panels. Under wind load, the mass of glass panels will apply inertia force on the cables in horizontal and vertical directions.

(2) Stiffness of Glass Panel. The stiffness of the glass panel includes the flexural stiffness of each glass panel and the membrane stress of the whole structure. Under the wind load, the deformation of cables is significant and nonuniform. The glass panel can reduce the deflection difference between the four corners and change the distribution of wind load. Like the statically indeterminate roof, the glass panel plays an important role in the transmission of wind loads and the deformation of the cables. On the other hand, since glass panels are connected by claws, there exists membrane stress on the entire glass wall. When glass panels deform under wind loads, the gap between the glass panel and claw is reduced and tension or compression force occurs in the connection of the glass panel and claw. In this way, all glass panels are effectively connected as a whole and thus influence the stiffness of the cables.

(3) Damping Effect of Glass Panels. A silicone sealant is used to glue each piece of glass and the buffering action of silicone and the friction between metal and rubber will weaken the vibration energy so as to increase the structural damping effect.

There are 21 vertical cables but no horizontal cables in the structure, with a cable spacing of 1.5 m. The length and cross area of the cable are 21 m and 1042 mm^2, respectively. The initial pretension of the cable is 300 kN. The type of glass panel is insulating-laminated glass and its specification is 10 + 12A + 8 + 1.52PVB + 8. The width of the sealant is 20 mm. This paper focuses on the out-of-plane deflection under wind load and the equivalent thickness is taken into account based on the assumption of equal deformation to simplify the calculation. Because the deflection under direct load is larger than the theoretical value, a reduction coefficient of 0.95 is adopted. So, the equivalent thickness of the glass panel can be calculated as $0.95 \times \sqrt{t_1^3 + t_2^3} = 0.95 \times \sqrt{10^3 + 17.52^3} =$

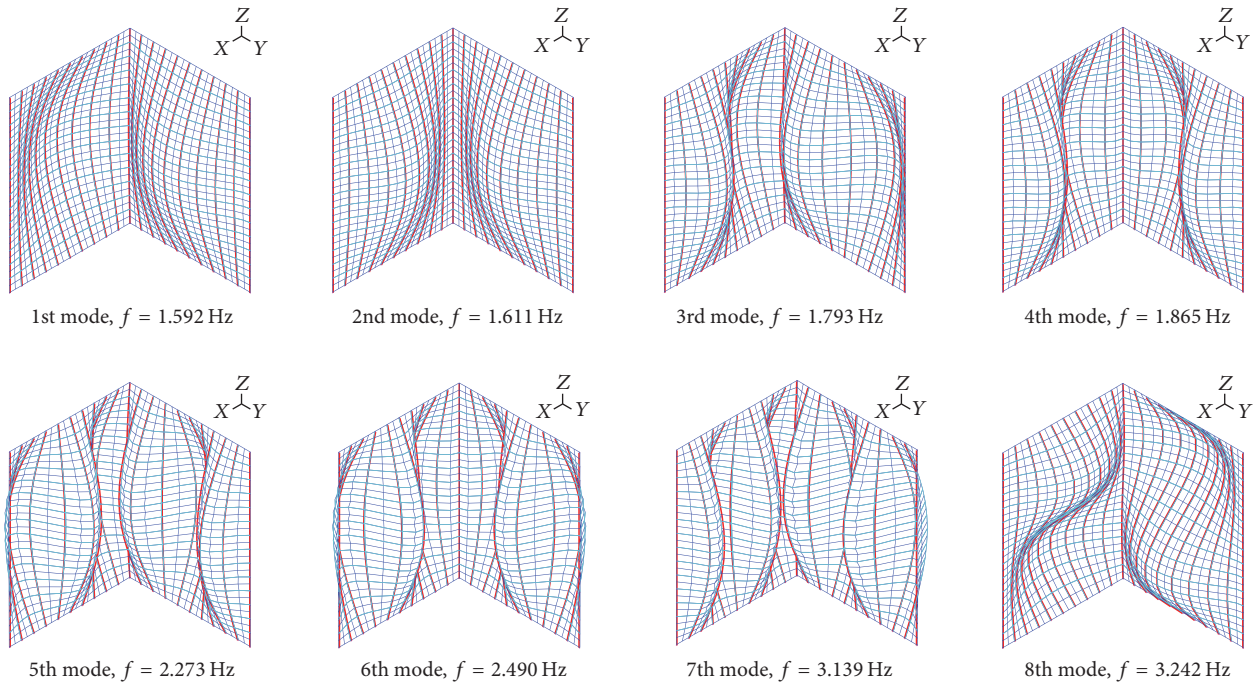

Figure 2: Vibration modes and frequencies of the structure.

Table 1: Mechanical properties of different components.

Component	Element type	Elastic modulus (Pa)	Poisson's ratio	Density (kg/m^3)
Cable	Truss	1.6e11	0.3	7850
Glass panel	Shell	7.2e10	0.23	2560
Sealant	Shell	3e6	0.48	500
Claw	Beam	2.06e11	0.3	7850

17.61 mm. In this paper, since the deflection of glass curtain under horizontal wind load is focused and the in-plane stiffness of glass panels is relatively larger, the effect of glass mass is ignored here and will be investigated in a future study.

The overall structural model is established by finite element software ADINA including glass panels, cables, connection claws, and sealants. Cables are simulated by truss element and hinged to the main structure, which can only bear axial force. Each cable is divided into 14 elements and the pretension is applied by initial strain. Claw connections are simulated by beam element. Both glass panels and sealants are simulated by shell element and each panel is divided into four elements. The mechanical properties of different components are presented in Table 1 and the structural damping ratio is taken as 0.02.

The dynamic characteristics of this structure are analyzed and the first 8 modes are shown in Figure 2. It can be illustrated that the structural stiffness is relatively small and the vibration frequencies and modes are densely distributed and coupled.

3. Numerical Simulation

In order to investigate the wind-induced response of the L-shaped cable support glass curtain structure, the time-domain method is adopted in numerical simulation, which includes simulations of wind flow and fluid-structure interaction. The fluctuating wind velocity time history is simulated by autoregressive linear filtering method based on the software MATLAB and the FSI is simulated by computational fluid dynamics software ADINA.

3.1. Fluctuating Wind Velocity Time History. Based on the period relationship between wind velocity and vibration of the structure, natural wind can be divided into two parts: mean wind with pulsation period of 10 min or longer and fluctuating wind with pulsation period of only a few seconds or even shorter. The mean wind velocity can be calculated by exponential distribution according to the *Load Code for the Design of Building Structures* [20] in China, as shown in Figure 3. Fluctuating wind can be approximated to be a Gaussian random process with zero mean, ergodicity, and spatial-temporal correlation. Since cross-wind and vertical-wind turbulence have a lower effect on structural deformation and are independent of each other, the along-wind dynamic response is mainly focused in this paper. Based on the Kaimal spectrum, random fluctuating wind velocity time history of different nodes can be simulated by the linear filtering technology, namely, autoregressive model (AR) in white-noise filtering method [21, 22].

The building is located in Fuzhou, China, where the site belongs to type B. The design wind pressure with 50-year return period is 0.7 and the design wind velocity is 33.5 m/s.

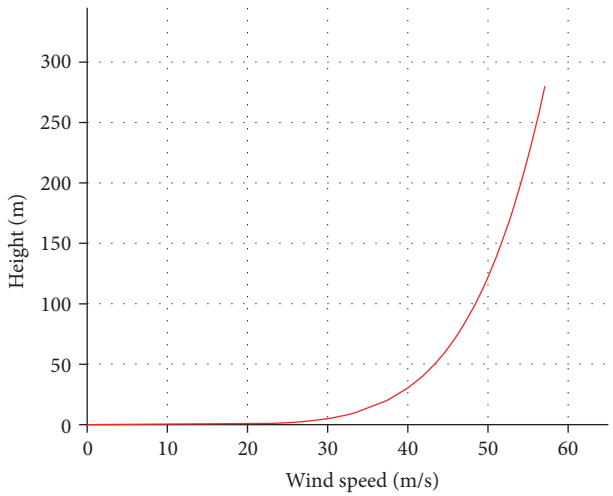

Figure 3: Average wind profile distribution.

According to the code, mean wind velocity in different heights can be determined by

$$\overline{U}_Z = \overline{U}_d \left(\frac{Z}{Z_d} \right)^{\alpha}, \tag{1}$$

where Z_d is the standard reference height and is taken as 10 m in the Chinese code; $\overline{U}_d$ is the mean wind speed at the height of Z_d and is set to be 33.5; α is the ground roughness exponent and is assumed to be 0.16.

Fluctuating wind can be simulated based on the Kaimal spectrum [23, 24]; namely,

$$\frac{nS_u(n)}{u^{*2}} = \frac{200f}{(1+50f)^{5/3}}, \tag{2}$$

where $f = nz/U(z)$; $u^* = KU(z)/\ln[z/z_0]$; $S_u(n)$ is the power spectrum of fluctuating wind velocity; n is the fluctuating wind frequency (Hz); z is the effective height; $U(z)$ is the mean wind speed at the height z; u^* is the air friction velocity; K is a dimensionless parameter and is taken as 0.4; z_0 is the length of ground roughness.

The fluctuating wind velocity time history can be expressed as

$$u(t) = \sum_{j=1}^{p} \psi_j u(t - j\Delta t) + N(t), \tag{3}$$

where p is the autoregressive order and is taken as 4; $N(t)$ is a series of stochastic processes with zero mean and an autocorrelation covariance matrix R; ψ_j $(j = 1, 2, \ldots, p)$ is the M-order matrix of autoregressive vector; and M is the number of simulated points.

$$R^{ik}(j\Delta t) = \int S_u^{ik}(n) \cos(2\pi j n \Delta t)\, dn, \tag{4}$$

where n is the fluctuating wind frequency (Hz) and S_u^{ik} is the autopower spectral density function of wind speed when $i = k$ and cross-power spectral density function when $i \neq k$; namely,

$$\begin{aligned} &S_u^{jk}(n) = \sqrt{S_u^{ii}(n) S_u^{kk}(n)}\, r_{ik}(n), \\ &r_{ik}(n) \\ &= \exp\left(\frac{-2n\sqrt{C_x^2 (x_i - x_k)^2 + C_y^2 (y_i - y_k)^2 + C_z^2 (z_i - z_k)^2}}{\overline{V}(z_i) + \overline{V}(z_k)} \right), \end{aligned} \tag{5}$$

where $r_{ik}(n)$ is the coherence function and C_x, C_y, and C_z are the attenuation coefficients between any two points in the directions of X, Y, and Z and are usually taken as 16, 8, and 10, respectively. (x_i, y_i, z_i) and (x_k, y_k, z_k) are the coordinates of points i and k. $\overline{V}(z_i)$ and $\overline{V}(z_k)$ are the mean wind velocity of points i and k.

$$R = \overline{R}\Psi, \tag{6}$$

where

$$\overline{R} = \begin{bmatrix} R(0) & R(\Delta t) & \cdots & R[(p-2)\Delta t] & R[(p-1)\Delta t] \\ R(\Delta t) & R(2\Delta t) & \cdots & R[(p-1)\Delta t] & R(0) \\ \vdots & \vdots & \ddots & \vdots & \vdots \\ R[(p-2)\Delta t] & R[(p-1)\Delta t] & \cdots & R[(p-4)\Delta t] & R[(p-3)\Delta t] \\ R[(p-1)\Delta t] & R(0) & \cdots & R[(p-3)\Delta t] & R[(p-2)\Delta t] \end{bmatrix},$$

$$R(j\Delta t) = \begin{pmatrix} R_{11}(j\Delta t) & R_{12}(j\Delta t) & \cdots & R_{1(M-1)}(j\Delta t) & R_{1M}(j\Delta t) \\ R_{21}(j\Delta t) & R_{22}(j\Delta t) & \cdots & R_{2(M-1)}(j\Delta t) & R_{2M}(j\Delta t) \\ \vdots & \vdots & \ddots & \vdots & \vdots \\ R_{(M-1)1}(j\Delta t) & R_{(M-1)2}(j\Delta t) & \cdots & R_{(M-1)(M-1)}(j\Delta t) & R_{(M-1)M}(j\Delta t) \\ R_{M1}(j\Delta t) & R_{M2}(j\Delta t) & \cdots & R_{M(M-1)}(j\Delta t) & R_{MM}(j\Delta t) \end{pmatrix},$$

$$\Psi = \left[\Psi_1^T, \ldots, \Psi_p^T\right]^T,$$
$$\Psi_j = \begin{bmatrix} \Psi_j^{11} & \cdots & \Psi_j^{1M} \\ \vdots & \ddots & \vdots \\ \Psi_j^{M1} & \cdots & \Psi_j^{MM} \end{bmatrix}. \tag{7}$$

The inlet boundary of flow field is divided into 36 regions and the center of each region is used to generate fluctuating wind speed time history according to the above method, with a total time of 100 s and an interval of 0.05 s. The fluctuating wind speed time history of all points in one region is consistent with that of the center point. Region division is shown in Figure 4. Taking regions (a), (b), and (c) as examples, comparison between their fluctuating wind speed time histories and the target Kaimal spectrum is presented in Figures 5 and 6. It can be seen that the simulated turbulent wind power spectrum can fit the target spectrum well. The wind speed time history in the inlet boundary can be obtained by the superposition of mean and fluctuating wind speed.

3.2. CFD Model. The computational domain can be divided into structural domain (CSD) and fluid domain (CFD). Based on the iterative coupling method, pressure and displacement can be exchanged on fluid-structure interaction surface between two domains until the computation is convergent. Fluid pressure from the CFD model can be transferred to the structure and leads to structural deformation. On the other hand, structural deformation can further change the distribution of fluid domain.

The size of fluid field is 450 m × 1200 m × 240 m and the blocking rate of cross-section wind is 3.4%. In order to meet the requirements of building shape and simulate the wind flow characteristics, the computing grids close to the structure should be small enough and densely distributed, while the grids away from the structure can be larger and sparse. The hexahedral element is adopted in fluid domain. The minimum scale of grids is 0.2 m at near-wall boundary and transits to far region with a rate of 1.2. A total of 850 thousand grids are generated in the whole region.

The generated wind speed time history is input at inlet boundary. The outlet boundary is set to be free boundary. Normal velocities on the sides and top surface are constrained. The ground surface and building surface adopt no-slip wall boundary. The fluid-structure coupling surface is specified on glass panels. The distance from the structure to inlet and outlet boundary is 400 m and 800 m, respectively, and the distance from the structure to both sides and the top of fluid field is 320 m and 240 m, respectively. The Smagorinsky model is adopted for large eddy simulation of the models [25–27].

According to structural symmetry, four wind directions, 0°, 15°, 30°, and 45°, are specified to analyze the structural response. Mesh generation of fluid model under different wind directions is shown in Figure 7.

3.3. Fluid-Structure Interaction. Structural model and fluid model were introduced in the previous sections. Due to the small stiffness, cable net glass curtain has large deformation under wind load and the fluid-structure interaction phenomenon is obvious. In order to reflect wind-induced vibration characteristics of an L-shaped cable net glass curtain wall, it is necessary to take fluid-structure interaction into consideration. An important feature of fluid-structure interaction (FSI) is the interaction between fluid and structure; namely, the structure deforms under fluid pressure but the structural deformation in turn affects the fluid flow, thereby changing the distribution and size of fluid pressure. Generally, there are two algorithms to solve FSI equation, namely, direct coupling method and iterative coupling method. In direct coupling method, all the physical quantities of structure, fluid, and interface are directly solved in one equation set. Though this method can be applied in most situations, its development is relatively slow because of the huge amount of calculation. Iterative coupling method, also known as partitioned method, separates the calculation into CFD and CSD, respectively, and realizes data exchange through fluid-structure interface until convergence. This method is adopted in this paper.

The basic criteria applied on FSI interface are kinematic conditions (also known as displacement compatibility) $\underline{d}_f = \underline{d}_s$ and dynamic conditions (also known as force balance) $n \cdot \underline{\tau}_f = n \cdot \underline{\tau}_s$, where $\underline{d}_f$ and $\underline{d}_s$ represent the displacement of fluid and structure, respectively, and $\underline{\tau}_f$ and $\underline{\tau}_s$ represent the stress of fluid and structure, respectively. The underline means that the values are only defined on FSI interface. The positions of nodes on FSI interface are determined by kinematic condition and the distributed force of fluid is applied to structural node in the form of concentrated force by the following integration:

$$F(t) = \int h^d \tau_f \, dS, \tag{8}$$

where h^d is the displacement of structural node.

Solution vector of the coupling system is expressed as $X = (X_f, X_s)$, where X_f and X_s are the solution vectors defined on nodes of fluid and structure, and $\underline{d}_s = \underline{d}_s(X_s)$, $\underline{\tau}_s = \underline{\tau}_s(X_f)$. Therefore, finite element equation of coupling system can be expressed as

$$F[X] \equiv \begin{bmatrix} F_f\left[X_f, \underline{d}_s(X_s)\right] \\ F_s\left[X_s, \underline{\tau}_f\left(X_f\right)\right] \end{bmatrix} = 0. \tag{9}$$

Since both fluid equations and FSI equations are nonlinear, the solving process is an iterative process that approximates the true solution gradually. During the iteration, the

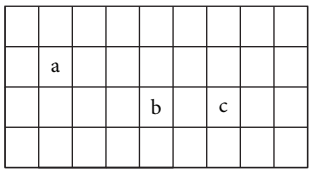

Figure 4: The divided regions of wind inlet boundary.

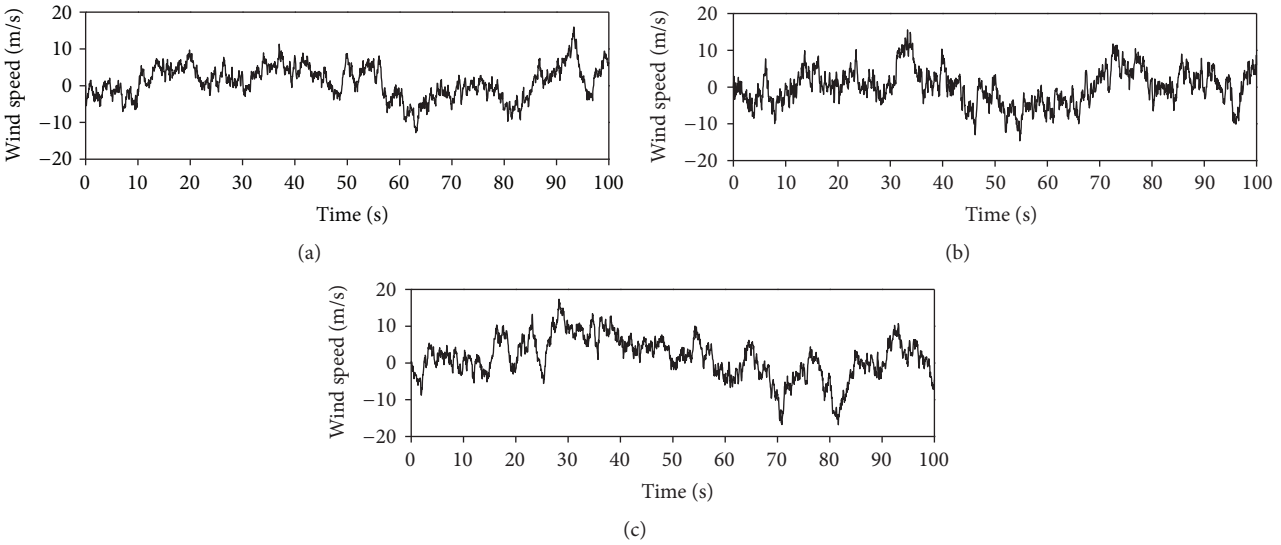

Figure 5: Fluctuating wind speed time histories in regions (a), (b), and (c).

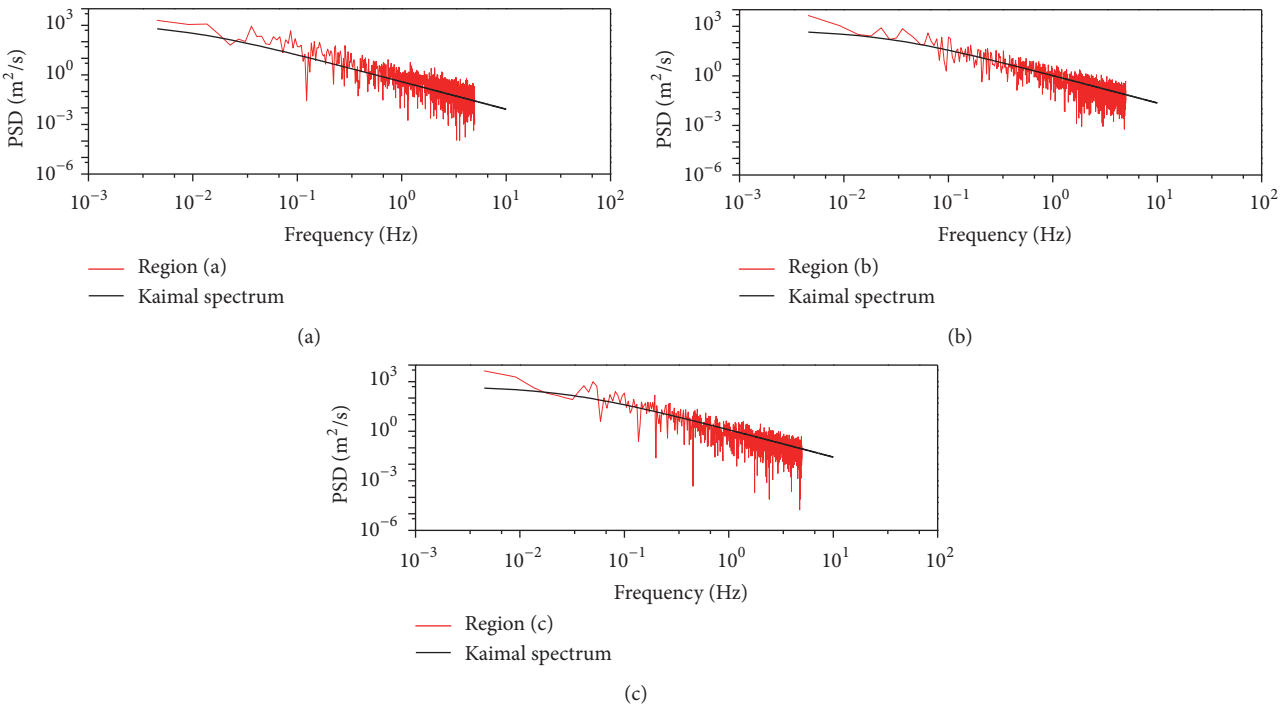

Figure 6: Comparison between target Kaimal spectrum and that computed with fluctuating wind speed time histories.

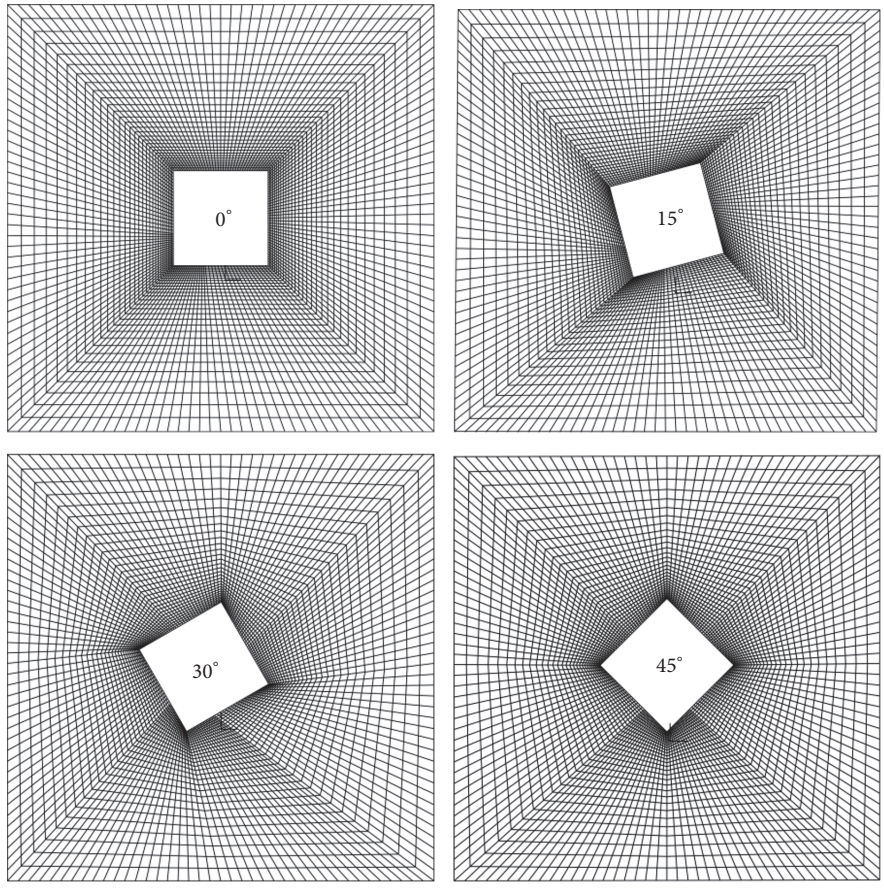

Figure 7: Mesh generation under different wind directions.

following criteria are used to estimate the convergence in terms of displacement and stress.

Displacement Criteria

$$r_d \equiv \frac{\left\| \underline{d}_s^k - \underline{d}_s^{k-1} \right\|}{\max\left\{ \left\| \underline{d}_s^k \right\|, \varepsilon_0 \right\}} \leq \varepsilon_d. \tag{10}$$

Stress Criteria

$$r_\tau \equiv \frac{\left\| \underline{\tau}_f^k - \underline{\tau}_f^{k-1} \right\|}{\max\left\{ \left\| \underline{\tau}_f^k \right\|, \varepsilon_0 \right\}} \leq \varepsilon_\tau, \tag{11}$$

where ε_τ and ε_d are the tolerances of stress and displacement convergence, respectively. ε_0 is the predetermined constant ($\varepsilon_0 = 10^{-8}$) to avoid small stress and displacement.

Structural displacement and fluid stress at time t are assumed to be $\underline{d}_s^{-1} = \underline{d}_s^0 = {}^t\underline{d}_s$ and $\underline{\tau}_s^0 = {}^t\underline{\tau}_f$ $\underline{d}_s^{-1} = \underline{d}_s^0 = {}^t\underline{d}_s$, $\underline{\tau}_s^0 = {}^t\underline{\tau}_f$. In order to obtain the solution at time $t+\Delta t$, iterative calculation between fluid model and structural model is carried out. The detailed computation steps for ${}^{t+\Delta t}X$ with iterative step k are introduced as follows.

(1) Based on the provided structural displacement, fluid solution vector X_f^k can be obtained by fluid equation $F_f[X_f^k, \lambda_d \underline{d}_s^{k-1} + (1-\lambda_d)\underline{d}_s^{k-2}] = 0$ and the fluid stress $\underline{\tau}_f^k$ can be further calculated as well. λ_d is the displacement relaxation factor. Then, check whether the residual stress of fluid field is smaller than the tolerance or not.

(2) Based on the fluid pressure on fluid-structure interface, structural solution vector X_s^k can be calculated through structural equation $F_s[X_s^k, \lambda_\tau \underline{\tau}_f^k + (1-\lambda_\tau)\underline{\tau}_f^{k-1}] = 0$ and then structural displacement $\underline{d}_s^k$ can be calculated. In structural equation, λ_τ is the stress relaxation factor.

(3) Based on structural displacement, the displacement of fluid node can be solved by $\underline{d}_f^k = \lambda_d \underline{d}_s^k + (1-\lambda_d)\underline{d}_s^{k-1}$.

(4) Verify whether residual stress and displacement meet the requirements or not. If not satisfied, return to the first step and continue to solve the variables iteratively until convergence. If the iterative steps exceed the upper limit, the program will automatically terminate and the solution is divergent.

The time step is set as $\Delta t = 0.05$ s and each time step is solved through the above-described process, so the displacement and stress distribution at all time steps can be obtained. The results calculated on FSI interface are applied on CSD model to calculate internal force and deformation of each element. The turbulence model used in CFD adopts LES-Smagorinsky model and the time integration formulation is

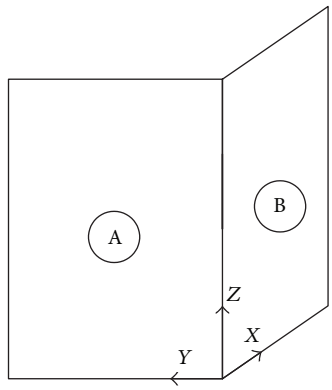

Figure 8: Definition of local coordinate system.

Bathe-Composite. The second-order spatial discretization is used and the fluid distribution and nodal location in fluid field are also adjusted accordingly.

4. Analysis of Results

The wind-induced response of cable support glass curtain wall is studied with consideration of fluid-structure interaction. Through cooperative work of flow field model and structural model, the wind-induced dynamic response within 100 s under four wind flow directions is obtained. The characteristics of wind-induced response are studied by statistical analysis of displacement, acceleration, and cable force.

4.1. Analysis of Displacement Response. In practical projects, equivalent static wind load is usually used to consider wind dynamic effect. Based on Davenport gust response theory, wind dynamic amplification effect can be expressed by wind vibration coefficient, namely, the ratio of the maximum response to the mean response. The equivalent static wind load is the product of static wind load and wind vibration coefficient.

By statistical analysis of displacement response of all nodes, displacement vibration coefficient β_{ndi} in different directions can be defined as

$$\beta_{ndi} = 1 + G\frac{\sigma_{u_{ndi}}}{\overline{u}_{ndi}}, \tag{12}$$

where the subscript ndi is denoted as node i; $\overline{u}_{ndi}$ is the mean value of nodal displacement; $\sigma_{u_{ndi}}$ is the mean square error of displacement; G is a peak factor and is set to 3.5 in this paper.

For the sake of discussion, local coordinate system of curtain wall structure is defined, where the vertical direction is the Z direction and both sides of the L-shaped structure are X direction and Y direction, respectively. Both glass surfaces are defined as surface A and surface B, respectively, as shown in Figure 8. The deformation in Z direction and in-plane deformation are ignored and this paper emphasizes the discussion of out-of-plane displacement in local coordinate system. Taking structural deformation at 20 s as an example, structural displacement under different wind directions is shown in Figure 9.

It can be seen that the maximum displacement at 20 s is 0.1788 m and the deformations of surface A and surface B are cooperative. The displacement is relatively large in the middle but relatively small in the edge. Under 0°, 15°, and 30° wind direction, the X direction displacement of surface A is positive and inward, while the Y direction displacement of surface B is positive and outward. In addition, there is a twist effect at the corner. However, under 45° wind direction, both surface A and surface B deform inward and show squeezing effect at the corner.

Since the displacement of middle points in both surfaces is relatively large and the corner deformation needs more attention, three middle points 1, 2, and 3 are taken as examples to analyze the out-of-plane displacement under different wind directions, as shown in Figure 10. The displacement time histories of these points are shown in Figure 11.

It can be found that, under four wind directions, displacement of point 1 is relatively large. The displacement of point 2 is relatively small but is significantly influenced by wind direction. Its Y direction displacement increases with the increase of wind direction. The out-of-plane displacement of point 3 also increases with the increase of wind direction.

Through statistical analysis, the maximum mean nodal displacement under 0°, 15°, 30°, and 45° wind direction is 0.147 m, 0.162 m, 0.160 m, and 0.159 m, respectively, while the maximum nodal displacement is 0.215 m, 0.238 m, 0.243 m, and 0.253 m, respectively.

In order to calculate displacement vibration coefficient, nine points on surface A and surface B are selected, respectively, as shown in Figure 12. The displacement vibration coefficients are calculated and presented in Tables 2 and 3, respectively. The results show that the displacement vibration coefficient of different points is comparative and changes little as the wind direction varies. This is because all nodes of glass curtain wall have strong synergetic deformation. The mean displacement vibration coefficient under 0°, 15°, 30°, and 45° wind direction is 1.807, 1.808, 1.830, and 1.995, respectively.

Since glass curtain wall has an envelope structure, based on the *Load Code for the Design of Building Structures* [20] and *Technical Specification for Glass Curtain Wall Engineering* [28], the vibration coefficient of this kind of structure is taken as 1.55, which is much smaller than the value computed in this paper. This is because the Chinese code adopts the inertia force method to calculate the wind vibration coefficient, in which the equivalent static wind load is expressed by the inertia force of first-order vibration mode of the structure. In general, this method is suitable for high-rise structures because its first-order vibration mode controls the response. However, it cannot meet the requirements of glass curtain wall due to structural flexibility, dense distribution of vibration frequencies, and coupled vibration modes. The displacement vibration coefficient can describe the dynamic amplification effect of fluctuating wind. According to the results of this study, the wind-induced vibration coefficient is suggested to be 2.0 for this kind of project.

4.2. Analysis of Acceleration Response. Taking the acceleration responses of points 1 and 3 under 0° and 45° wind direction as examples (Figure 10), frequency-domain analysis

Table 2: Displacement vibration coefficients of points on surface A.

Wind direction	A1	A2	A3	A4	A5	A6	A7	A8	A9
0°	1.8228	1.801	1.8861	1.8009	1.7949	1.8523	1.839	1.8175	1.9155
15°	1.7756	1.7157	1.7572	1.7511	1.7057	1.7248	1.7872	1.7248	1.7723
30°	1.7995	1.7991	1.7677	1.7743	1.7879	1.7298	1.8102	1.7055	1.7791
45°	2.1511	1.9407	2.0451	2.1160	1.9361	1.9948	2.1693	1.9496	2.0633

Table 3: Displacement vibration coefficients of points on surface B.

Wind direction	B1	B2	B3	B4	B5	B6	B7	B8	B9
0°	1.7179	1.8056	1.8283	1.7086	1.8033	1.8225	1.7103	1.7931	1.8144
15°	1.7866	1.8303	1.9151	1.7619	1.9274	2.0167	1.7748	1.9218	1.9013
30°	1.8064	1.8429	1.9477	1.7709	1.9164	1.9876	1.8421	1.9163	1.9547
45°	1.9527	1.8586	2.0336	1.908	1.8461	2.0056	1.9684	1.8385	2.1385

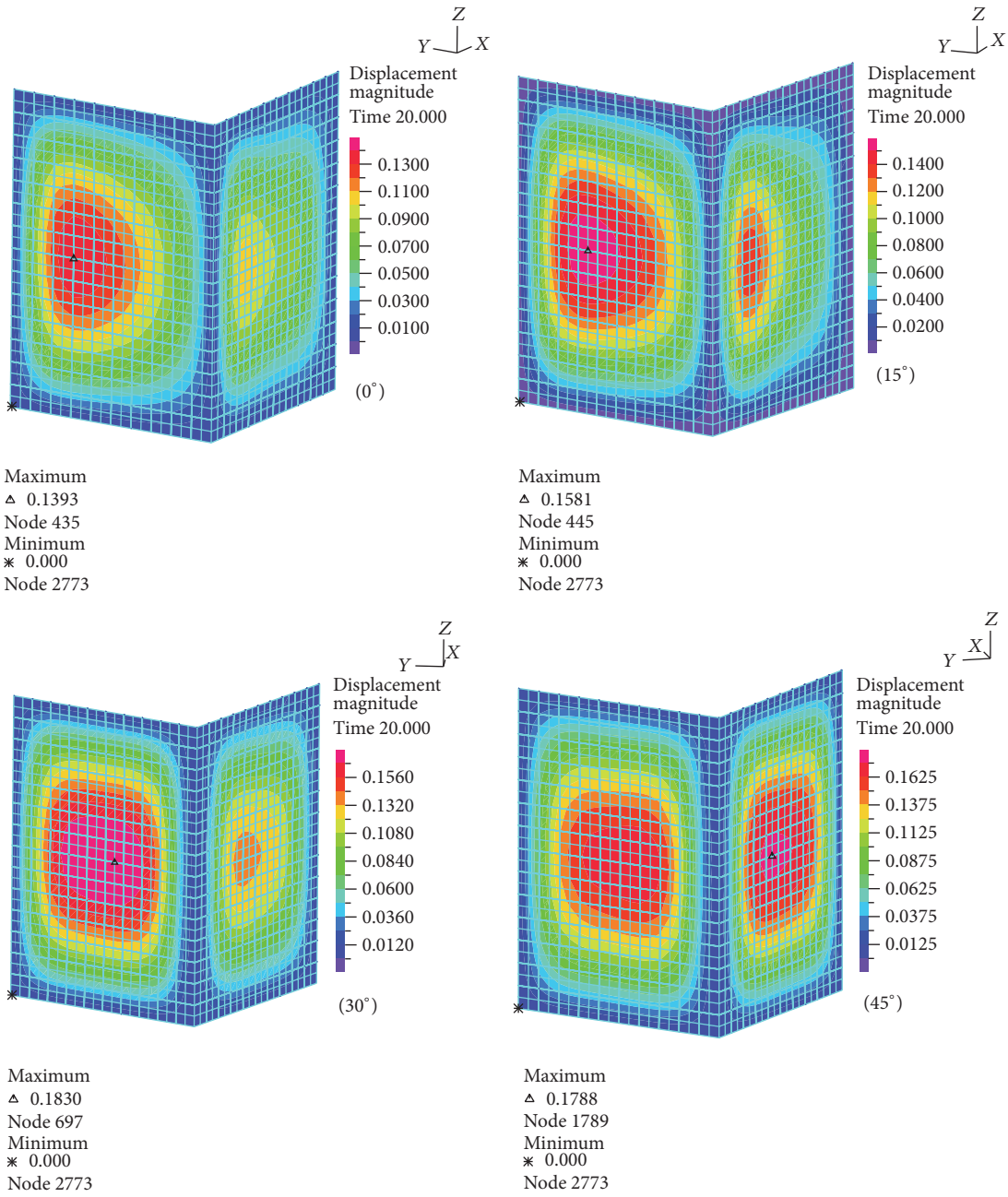

Figure 9: Structural displacement at $t = 20$ s under different wind directions.

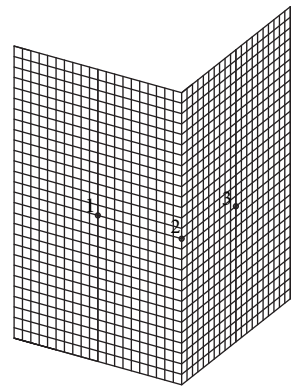

Figure 10: The locations of selected points.

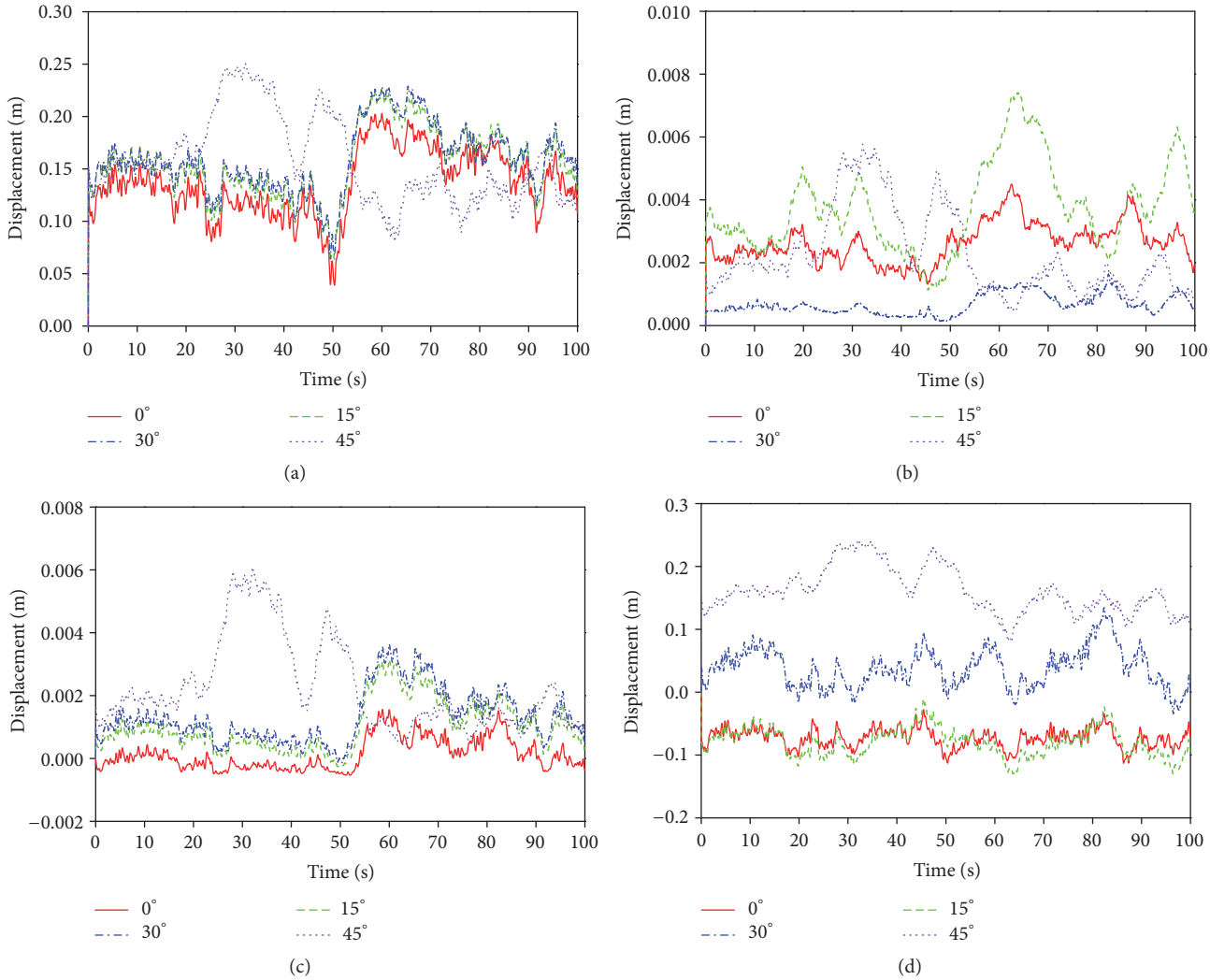

Figure 11: Displacement results: (a) X displacement of point 1; (b) X displacement of point 2; (c) Y displacement of point 2; (d) Y displacement of point 3.

of acceleration time history in points 1 and 3 is carried out, as shown in Figures 13 and 14.

Compared with structural dynamic characteristics, acceleration power spectrum shows that the first few modes of the structure are from 1.5 Hz to 2.5 Hz, which proves that the acceleration response is mainly affected by low-order modes and the influence of high-order modes is small. Due to dense frequency distribution, it is difficult to select the number of

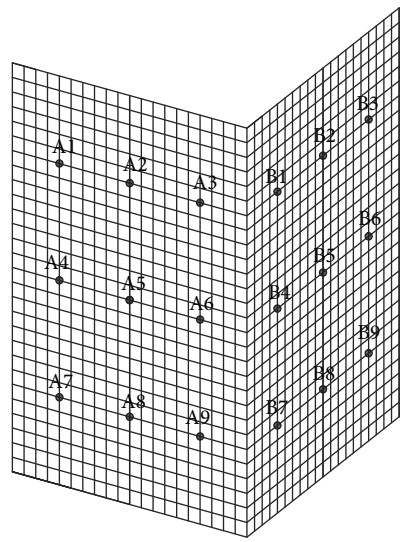

Figure 12: Location of points selected for calculation of displacement vibration coefficient.

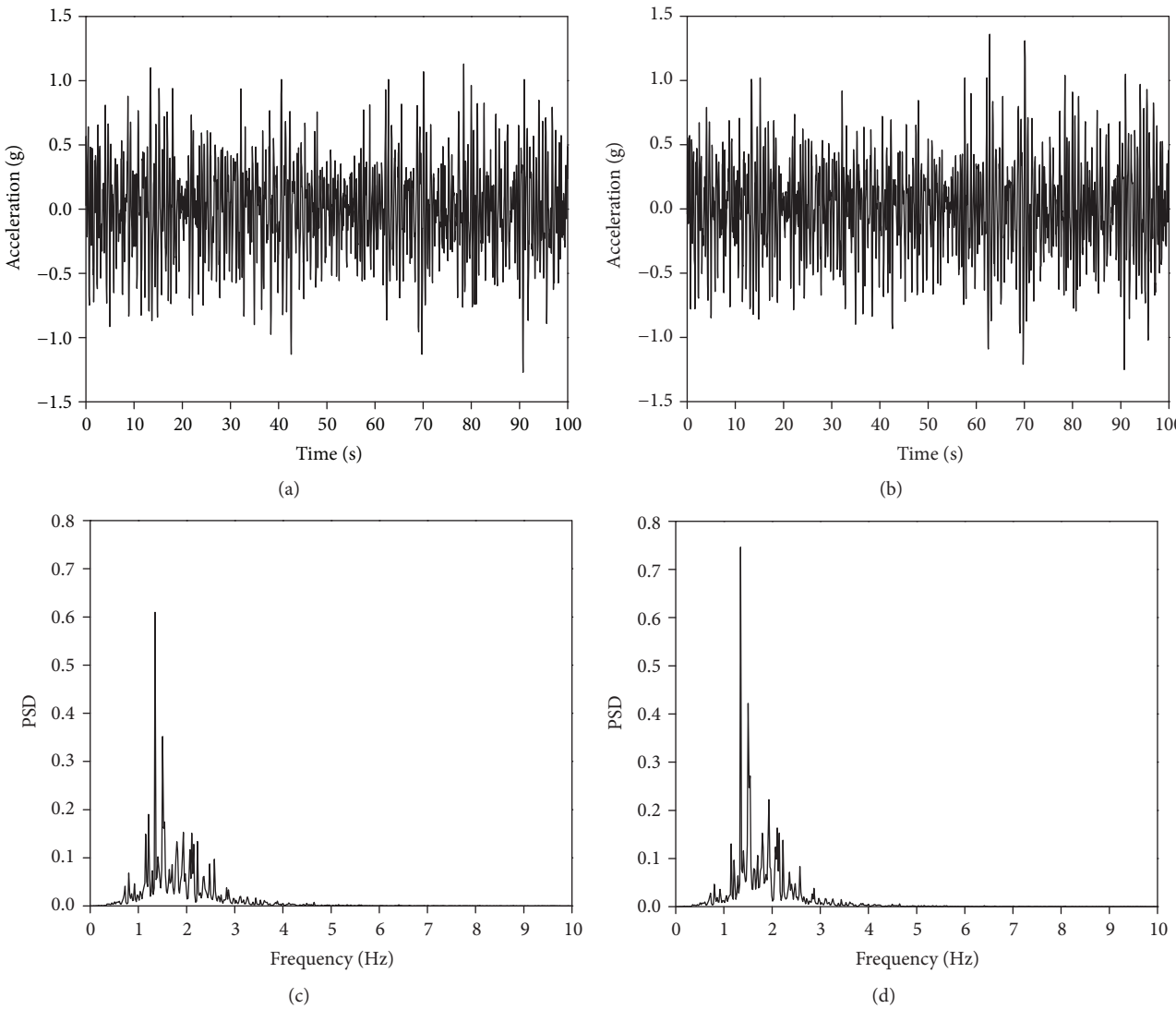

Figure 13: Acceleration results under 0° wind direction: (a) X acceleration of point 1; (b) Y acceleration of point 3; (c) power spectral density of point 1; (d) power spectral density of point 3.

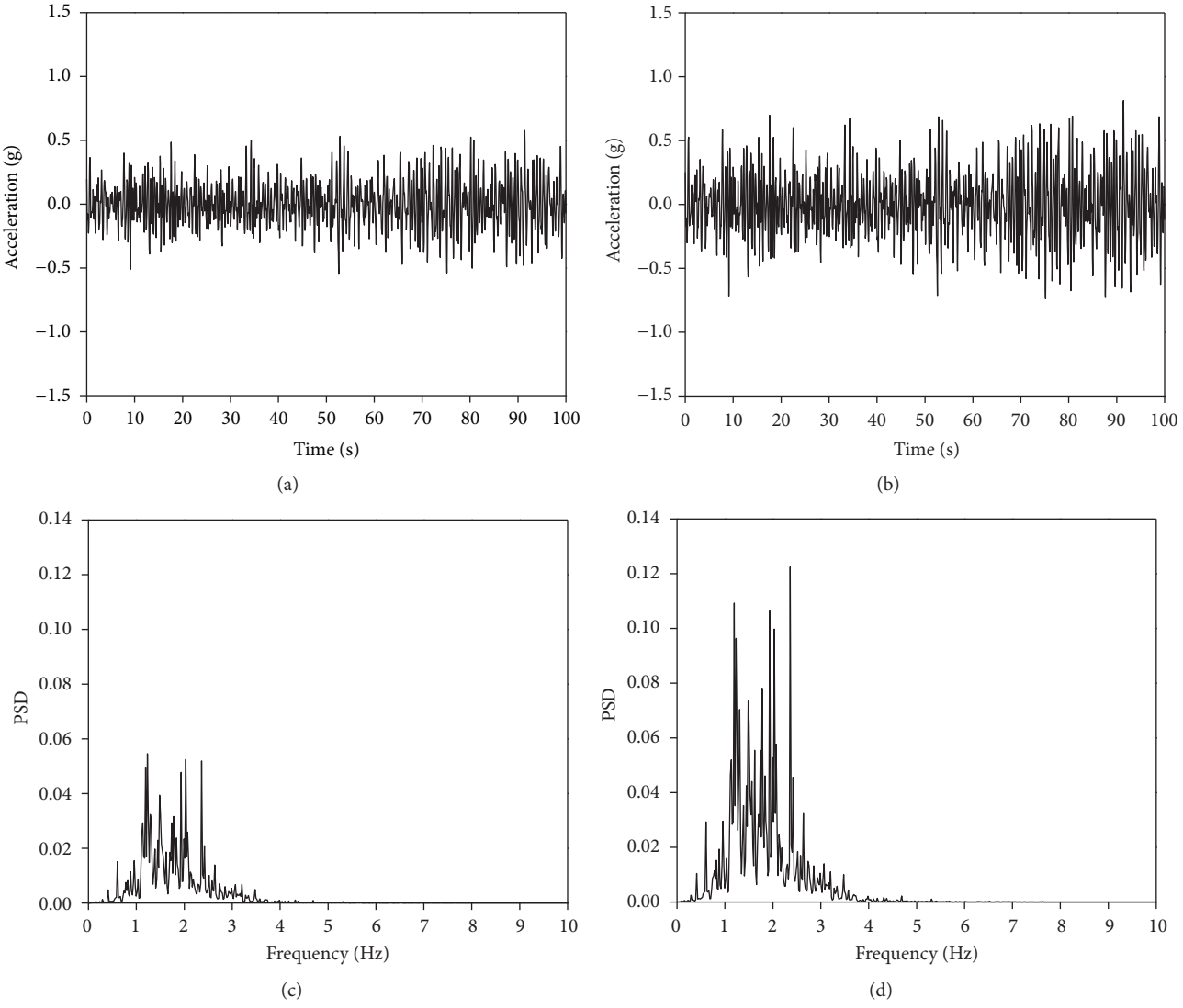

Figure 14: Acceleration results under 45° wind direction: (a) X acceleration of point 1; (b) Y acceleration of point 3; (c) power spectral density of X acceleration of point 1; (d) power spectral density of Y acceleration of point 3.

computing modes in frequency-domain analysis method and this paper adopts time-domain analysis method. Through comparison of acceleration time histories, it can be concluded that wind direction has few influences on the acceleration response.

4.3. Analysis of Cable Force Results. There are only vertical cables in this project with prestress of 300 kN. The elevation span of the cables is from 42 m to 63 m. The cables are labeled from 1 to 11 on surface A and 11 to 21 on surface B, as shown in Figure 15. In other words, the cable at the corner is labeled as 11. The statistics of mean axial force of each cable under each wind direction are assessed and shown in Figure 16.

It can be seen that, under 0° wind direction, cable force is large in the middle and small at both ends on surface A, but the situation is opposite on surface B. The maximum mean cable force is 344 kN in cable 13. The distribution of cable force under 15° wind direction is similar to that under 0° wind direction. The axial force of cables increases on surface B but decreases on surface A, with the maximum mean axial force of 357 kN in cable 13. Under 30° wind direction, the mean force of different cables decreases. The axial force on surface A has little change, while that on surface B increases in the middle and decreases in the end, with the maximum mean axial force of 338 kN in cable 5. Under 45° wind direction, the axial force on surfaces A and B is similar and the maximum mean axial force is 339 kN in cable 15.

The results show that, in limit states of serviceability, the wind-induced vibration does not lead to obvious stiffness degradation. The structure has strong overall coordination and the maximum axial force appears in the central upper part due to height variation of wind pressure. In addition, distribution of axial force on surface A and surface B has a significant difference because of the wind flow characteristics around the structure. As the wind direction increases, the axial force of cables on surface B increases as well.

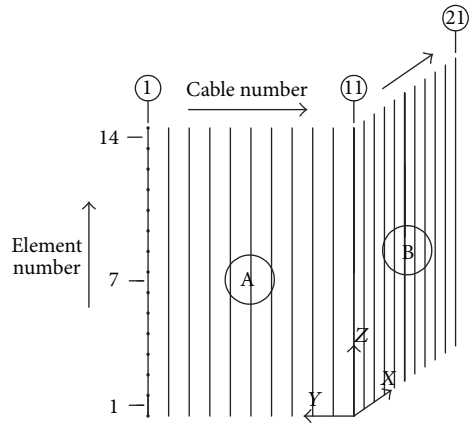

Figure 15: Number labels of cable and truss element.

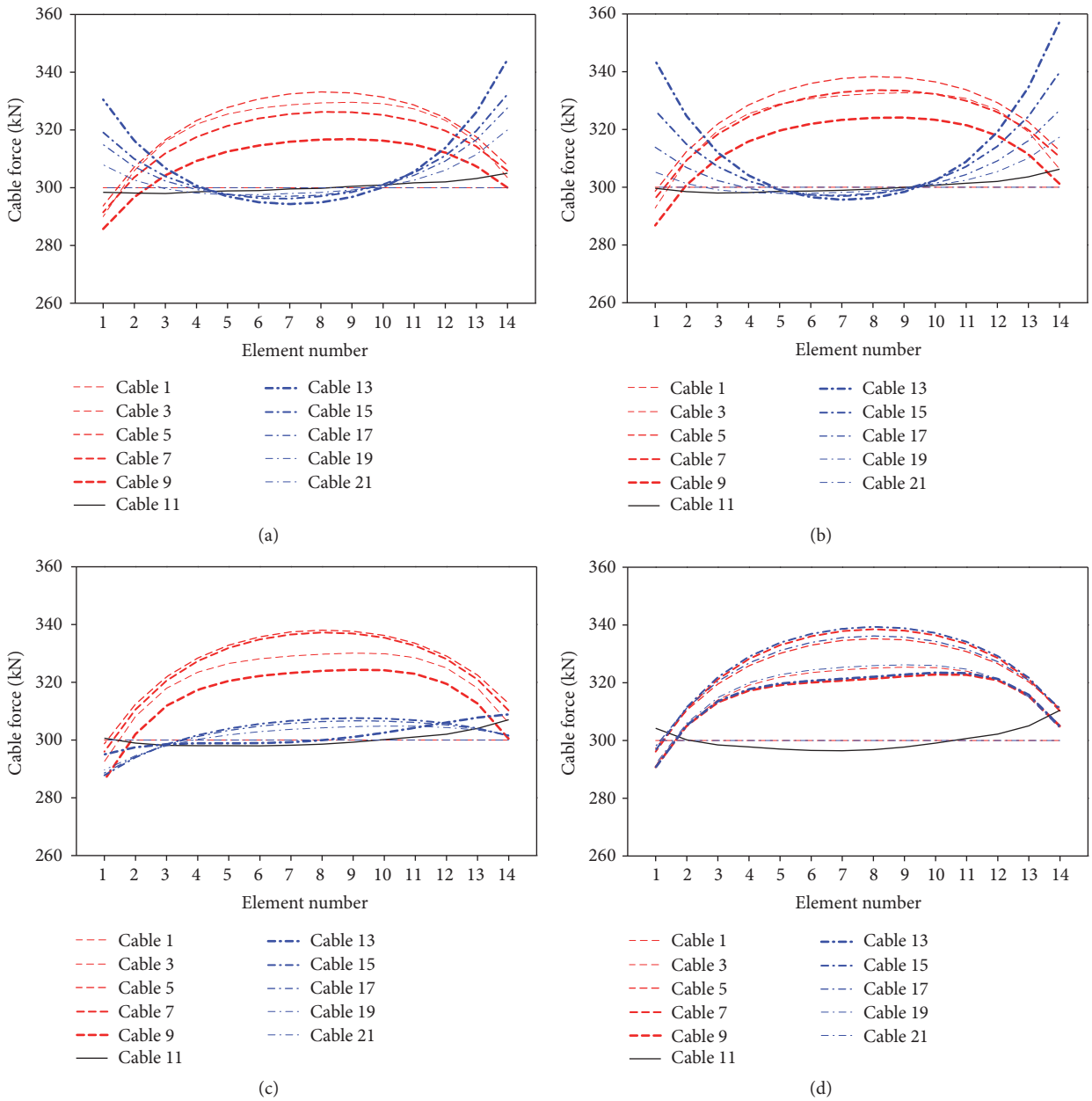

Figure 16: Mean cable force under different wind directions: (a) 0°, (b) 15°, (c) 30°, and (d) 45°.

5. Conclusions

At present, the study on wind-induced response of an L-shaped cable support glass curtain wall is still in the initial stage. In this paper, wind-induced response of an L-shaped cable support glass curtain wall is analyzed under different wind directions by time-domain method with consideration of fluid-structure interaction effect. The dynamic response of glass surface is studied by statistical analysis of displacement, acceleration, and cable force. Based on the obtained results, the following conclusions can be drawn.

(1) The maximum displacement of the structure is 0.253 m under 45° wind direction. The glass curtain wall shows strong integrity and deforms cooperatively. The wind-induced vibration coefficient is suggested to be 2.0 for practical projects, which will result in conservative results when compared with Chinese codes. The displacement at the corner is relatively small, indicating that the stiffness of both surfaces is large enough.

(2) Through analysis of acceleration time history and power spectrum, under fluctuating wind load, the first few modes are excited and the vibration of this structure is a narrow-band process.

(3) The analysis of cable axial force shows that the maximum mean axial force can reach 357 kN. The distribution of axial force on both surfaces is quite different and is significantly affected by the wind direction.

This study mainly focuses on L-shaped single-layer curtain walls with vertical cables and more studies are required on the structure with vertical and horizontal cables. Besides, if the frequency-domain method is used, how to select the number of vibration modes and consider their coupling effect should be discussed in the future study.

Conflicts of Interest

The authors declare that there are no conflicts of interest regarding the publication of this paper.

References

[1] M. A. Vyzantiadou and A. V. Avdelas, "Point fixed glazing systems: Technological and morphological aspects," *Journal of Constructional Steel Research*, vol. 60, no. 8, pp. 1227–1240, 2004.

[2] T. Moschner, J. Schlaich, and H. Schober, "Prestressed cable-net facades," *Structural Engineering International*, vol. 15, no. 1, pp. 36–39, 2005.

[3] R.-Q. Feng, L.-L. Zhang, Y. Wu, and S.-Z. Shen, "Dynamic performance of cable net facades," *Journal of Constructional Steel Research*, vol. 65, no. 12, pp. 2217–2227, 2009.

[4] R.-Q. Feng, J.-H. Ye, Y. Wu, and S.-Z. Shen, "Nonlinear response spectra of cable net facades," *Soil Dynamics and Earthquake Engineering*, vol. 32, no. 1, pp. 71–86, 2012.

[5] C. Amadio and C. Bedon, "Viscoelastic spider connectors for the mitigation of cable-supported façades subjected to air blast loading," *Engineering Structures*, vol. 42, pp. 190–200, 2012.

[6] C. Bedon and C. Amadio, "Exploratory numerical analysis of two-way straight cable-net façades subjected to air blast loads," *Engineering Structures*, vol. 79, pp. 276–289, 2014.

[7] Z.-Q. Zhang, Y.-L. Ding, and F.-F. Geng, "Investigation of influence factors of wind-induced buffeting response of a six-tower cable-stayed bridge," *Shock and Vibration*, vol. 2016, Article ID 6274985, 16 pages, 2016.

[8] F. Xu, C. Li, and T. Jiang, "On the shaker simulation of wind-induced non-gaussian random vibration," *Shock and Vibration*, vol. 2016, Article ID 5450865, 10 pages, 2016.

[9] C. L. Lu, Q. S. Li, S. H. Huang, A. Y. Tuan, L. H. Zhi, and S.-C. Su, "Evaluation of wind loads and wind induced responses of a super-tall building by large eddy simulation," *Wind and Structures*, vol. 23, no. 4, pp. 313–350, 2016.

[10] L. L. Wu, Y. J. Shi, and Y. Q. Wang, "Wind-induced response characteristics of monolayer cable net," *Journal of Engineering Mechanics*, vol. 136, no. 3, Article ID 002003QEM, pp. 311–321, 2010.

[11] Z.-D. Xu, J.-T. Zhu, and D.-X. Wang, "Analysis and optimisation of wind-induced vibration control for high-rise chimney structures," *International Journal of Acoustics and Vibrations*, vol. 19, no. 1, pp. 42–51, 2014.

[12] Z. W. Zhao, Z. H. Chen, X. D. Wang, X. Hao, and H. B. Liu, "Wind-induced response of large-span structures based on pod-pseudo-excitation method," *Advanced Steel Construction*, vol. 12, no. 1, pp. 1–16, 2016.

[13] W. Hernandez, J. L. Maldonado-Correa, and A. Méndez, "Frequency-domain analysis of performance of a wind turbine," *Electronics Letters*, vol. 52, no. 3, pp. 221–223, 2016.

[14] R. Liu, C. Huang, and Z. Huo, "Dynamic response of the glass curtain wall of the cable truss under wind loads," in *Proceedings of the Global Conference on Civil, Structural and Environmental Engineering/3rd International Symp on Multi-field Coupling Theory of Rock and Soil Media and its Applications, Advanced Materials Research*, vol. 594–597, pp. 921–924, Yichang, China, October 2012.

[15] R. Q. Feng, Y. Wu, and S. Z. Shen, "A simplified calculating method of nonlinear frequency of cable net under mean wind load," *Acta Mechanica Solida Sinica*, vol. 19, no. 3, pp. 248–254, 2006.

[16] X. L. Zhang and Y. Z. Ju, "Analysis of wind-induced vibration response on tower consisted of steel tubes and angle steels," in *Proceedings of the 14th International Symposium on Structural Engineering (ISSE-14), Fundamental Research in Structural Engineering: Retrospective and Prospective*, vol. 1-2, pp. 891–896, Beijing , China, October 2016.

[17] L. M. Zhang, W. J. Chen, and S. L. Dong, "Natural vibration and wind-induced response analysis of the non-fully symmetric Geiger cable dome," *Journal of Vibroengineering*, vol. 16, no. 1, pp. 31–41, 2014.

[18] J. G. Cai, J. Feng, L. F. Huang, and H. B. Cao, "Study on wind-induced vibration of single-layer cable net supported glass curtain walls," in *Proceedings of the 10th International Symposium on Structural Engineering for Young Experts*, vol. i-ii, pp. 1655–1660, Changsha, China, October 2008.

[19] Y. Wang, L. Wu, Y. Shi, F. Sun, K. Luo, and V. Xu, "FEM analysis and experimental study on monolayer cable net for glass facades: Static performance," *Advances in Structural Engineering*, vol. 10, no. 4, pp. 371–382, 2007.

[20] GB 50009-2001, "Load code for the design of building structures".

[21] J. S. Owen, B. J. Eccles, B. S. Choo, and M. A. Woodings, "The application of auto-regressive time series modelling for the: time-frequency analysis of civil engineering structures," *Engineering Structures*, vol. 23, no. 5, pp. 521–536, 2001.

[22] A. G. Poulimenos and S. D. Fassois, "Parametric time-domain methods for non-stationary random vibration modelling and analysis—a critical survey and comparison," *Mechanical Systems and Signal Processing*, vol. 20, no. 4, pp. 763–816, 2006.

[23] L. Tian and Y. Zeng, "Parametric study of tuned mass dampers for long span transmission tower-line system under wind loads," *Shock and Vibration*, vol. 2016, Article ID 4965056, 11 pages, 2016.

[24] M. Wu, Y. Li, X. Chen, and P. Hu, "Wind spectrum and correlation characteristics relative to vehicles moving through cross wind field," *Journal of Wind Engineering and Industrial Aerodynamics*, vol. 133, pp. 92–100, 2014.

[25] C. Bogey and C. Bailly, "Large eddy simulations of round free jets using explicit filtering with/without dynamic Smagorinsky model," *International Journal of Heat and Fluid Flow*, vol. 27, no. 4, pp. 603–610, 2006.

[26] J. Meyers and P. Sagaut, "On the model coefficients for the standard and the variational multi-scale Smagorinsky model," *Journal of Fluid Mechanics*, vol. 569, pp. 287–319, 2006.

[27] E. Zhang, L. Hou, H. Cai, C. Shen, and Y. Zhang, "Research on thermal-field and sound-field coupling properties of different grid forms," *Shock and Vibration*, vol. 2016, Article ID 2741748, 10 pages, 2016.

[28] JGJ 102-2003, "Technical Specification of Glass Curtain Wall Engineering".